



Resistive and ferritic-wall plasma dynamos in a sphere

I. V. Khalzov, B. P. Brown, E. J. Kaplan, N. Katz, C. Paz-Soldan et al.

Citation: [Phys. Plasmas](#) **19**, 104501 (2012); doi: 10.1063/1.4757219

View online: <http://dx.doi.org/10.1063/1.4757219>

View Table of Contents: <http://pop.aip.org/resource/1/PHPAEN/v19/i10>

Published by the [American Institute of Physics](#).

Additional information on Phys. Plasmas

Journal Homepage: <http://pop.aip.org/>

Journal Information: http://pop.aip.org/about/about_the_journal

Top downloads: http://pop.aip.org/features/most_downloaded

Information for Authors: <http://pop.aip.org/authors>

ADVERTISEMENT

The advertisement features a green and white abstract background of flowing lines. At the top, the 'AIP Advances' logo is displayed, with 'AIP' in blue and 'Advances' in green, accompanied by a series of orange and yellow dots. Below the logo, the text 'Special Topic Section:' is written in white, followed by 'PHYSICS OF CANCER' in large, bold, white capital letters. At the bottom, the phrase 'Why cancer? Why physics?' is written in white, and a blue button with the text 'View Articles Now' is positioned to the right.

Resistive and ferritic-wall plasma dynamos in a sphere

I. V. Khalzov,^{1,2} B. P. Brown,^{1,2} E. J. Kaplan,^{1,2} N. Katz,^{1,2} C. Paz-Soldan,^{1,2}
 K. Rahbarnia,^{1,2} E. J. Spence,^{2,3} and C. B. Forest^{1,2}

¹University of Wisconsin-Madison, 1150 University Avenue, Madison, Wisconsin 53706, USA

²Center for Magnetic Self Organization in Laboratory and Astrophysical Plasmas, USA

³Princeton Plasma Physics Laboratory, P.O. Box 451, Princeton, New Jersey 08543, USA

(Received 1 April 2012; accepted 18 September 2012; published online 10 October 2012)

We numerically study the effects of varying electric conductivity and magnetic permeability of the bounding wall on a kinematic dynamo in a sphere for parameters relevant to Madison plasma dynamo experiment. The dynamo is excited by a laminar, axisymmetric flow of von Kármán type. The flow is obtained as a solution to the Navier-Stokes equation for an isothermal fluid with a velocity profile specified at the sphere's boundary. The properties of the wall are taken into account as thin-wall boundary conditions imposed on the magnetic field. It is found that an increase in the permeability of the wall reduces the critical magnetic Reynolds number Rm_{cr} . An increase in the conductivity of the wall leaves Rm_{cr} unaffected but reduces the dynamo growth rate. © 2012 American Institute of Physics. [<http://dx.doi.org/10.1063/1.4757219>]

Over the past decade, significant effort has been directed at the experimental demonstration of dynamo action—self-excitation and maintenance of the magnetic field in a flowing electrically conducting fluid. A number of experiments with liquid metals have been constructed to test this phenomenon in various settings,^{1–6} and successful observations of dynamo action have been reported in three of them.^{4–6} These experiments revealed the critical importance of the magnetic properties of the flow-driving impellers. Namely, the von Kármán sodium experiment only self-sustained a dynamo field if the impellers were ferromagnetic.^{6,7} In addition, the finite resistivity of the experimental container is expected to be crucial for the dynamo instability—a situation similar to the resistive wall mode (RWM) in tokamaks.⁸ Normally stable for the perfectly conducting wall, the RWM can become unstable if the wall has finite resistivity and the instability develops on the wall's resistive time scale. These facts initiated more thorough theoretical studies of the effect of the imposed boundary conditions on the dynamo in experimentally relevant models.^{9–16} The studies established that there are no general dependences of dynamo properties on conductivity and permeability of the boundary; the dependences are different for different models and flows.

This circumstance motivates us to perform an analogous study for the Madison plasma dynamo experiment (MPDX, Fig. 1), currently under construction at the University of Wisconsin-Madison. The experiment is aimed at investigations of dynamos excited by controllable flows of plasmas. Its original design was proposed in Refs. 17 and 18, and conceptual features were successfully tested in the plasma Couette experiment (PCX).¹⁹ The experimental vessel is a sphere of 3 m in diameter. An axisymmetric multicusp magnetic field confines the plasma. The field is localized near the vessel wall and a large volume of unmagnetized plasma occupies the experiment's core. An electric field applied across the multicusp field drives the edge of the plasma azimuthally. Arbitrary profiles of azimuthal flow $v_\phi(\theta)$ can be imposed at the spherical boundary by modulating the

electric field as a function of polar angle θ using discrete electrodes.

Results of Ref. 18 show that flows generated in such a way can lead to a dynamo. However, in Ref. 18, insulating boundaries are assumed, whereas in MPDX, the vessel is made of aluminum whose conductivity is much higher than that of the plasma under expected conditions. The goal of this paper is to consider effects of varying conductivity and permeability of the vessel on the dynamo.

To describe the plasma, we use dimensionless numbers

$$M = V_0 \sqrt{\frac{\rho_0}{P_0}}, \quad Re = \frac{R_0 V_0}{\nu}, \quad Rm = \frac{R_0 V_0}{\eta}, \quad Pm = \frac{\nu}{\eta},$$

Mach, fluid Reynolds, magnetic Reynolds, and magnetic Prandtl, respectively. Here V_0 is the peak driving velocity, ρ_0 and P_0 are the average plasma mass density and pressure, R_0 is the radius of the sphere (a unit of length throughout the paper), ν and η are the plasma kinematic viscosity and magnetic diffusivity (assumed to be constant and uniform). For given plasma parameters, these numbers can be estimated from the Braginskii equations²⁰ (see corresponding formulas in Refs. 18 and 21). Their expected values for MPDX are listed in Table I. By varying temperature, density, and ion species of the plasma, one can change its magnetic Prandtl number by several orders of magnitude. Such flexibility makes it possible to demonstrate a dynamo in a laminar flow by choosing a regime with $Pm \sim 1$ and $Rm \sim Re \sim 10^2$.

Our first step is to find an equilibrium velocity field capable of dynamo action. For simplicity, we do not focus on the details of plasma driving near the wall. We neglect the multicusp magnetic field and applied electric field and assume that the velocity profile is specified at the boundary. As shown in Ref. 21 for the model relevant to PCX (cylindrical prototype of MPDX), the velocity structure obtained under such assumption is the same as that obtained with a more realistic $\mathbf{E} \times \mathbf{B}$ forcing, except in a thin boundary layer.

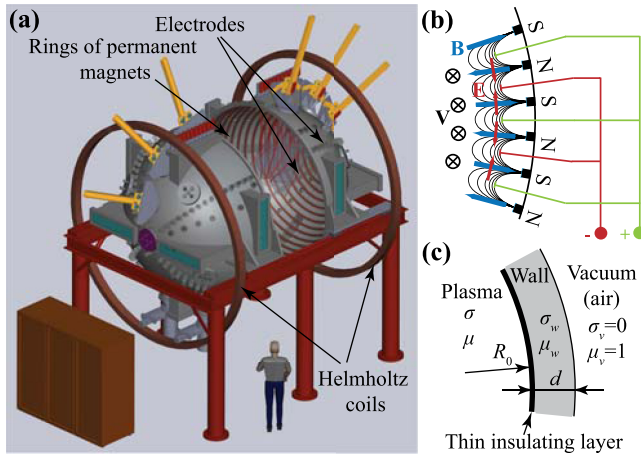


FIG. 1. Madison plasma dynamo experiment (MPDX): (a) sketch of the experiment; (b) electrode configuration near the wall for driving plasma velocity $v_\phi(\theta)$; (c) model for deriving thin-wall boundary conditions, with σ and μ denoting conductivity and relative permeability of the respective media. (b) is reproduced by permission from Spence *et al.*, *Astrophys. J.* **700**, 470 (2009). Copyright 2009 by AAS.

The velocity field is found using the hydrodynamic part of the extended MHD code NIMROD²² with an isothermal fluid model, which in non-dimensional form is

$$\frac{\partial n}{\partial \tau} = -\nabla \cdot (n\mathbf{v}), \quad (1)$$

$$n \frac{\partial \mathbf{v}}{\partial \tau} = -n(\mathbf{v} \cdot \nabla)\mathbf{v} - \frac{\nabla n}{M^2} + \frac{1}{Re} \left(\nabla^2 \mathbf{v} + \frac{1}{3} \nabla(\nabla \cdot \mathbf{v}) \right), \quad (2)$$

where τ , n , and \mathbf{v} stand for normalized time, density and velocity, respectively: $\tau = tV_0/R_0$, $n = \rho/\rho_0$, $\mathbf{v} = \mathbf{V}/V_0$. The differential plasma driving at the boundary is

$$\mathbf{v}|_{r=1} = v_\phi(\theta)\mathbf{e}_\phi, \quad 0 \leq \theta \leq \pi, \quad (3)$$

where $v_\phi(\theta)$ is a function of polar angle θ with physical restriction $v_\phi(0) = v_\phi(\pi) = 0$. In general, it may be expressed as $v_\phi(\theta) = \sum a_k \sin k\theta$. We use a velocity boundary condition of the von Kármán type from Ref. 18, shown to result in a dynamo. It is given by $a_2 = -0.4853$, $a_4 = -0.5235$, $a_6 = -0.0467$, $a_8 = 0.1516$ (Fig. 2(a)). We take the Mach number $M=1$, the fluid Reynolds number

TABLE I. Expected parameters of MPDX.

Quantity	Symbol	Value	Unit
Radius of sphere	R_0	1.5	m
Wall thickness	d	0.05	m
Peak driving velocity	V_0	0–20	km/s
Average number density	n_0	$10^{17} - 10^{19}$	m^{-3}
Electron temperature	T_e	2–10	eV
Ion temperature	T_i	0.5–4	eV
Ion species		H, He, Ne, Ar	
Ion mass	μ_i	1, 4, 20, 40	amu
Mach	M	0–8	
Fluid Reynolds	Re	$0 - 10^5$	
Magnetic Reynolds	Rm	$0 - 2 \times 10^3$	
Magnetic Prandtl	Pm	$10^{-3} - 5 \times 10^3$	

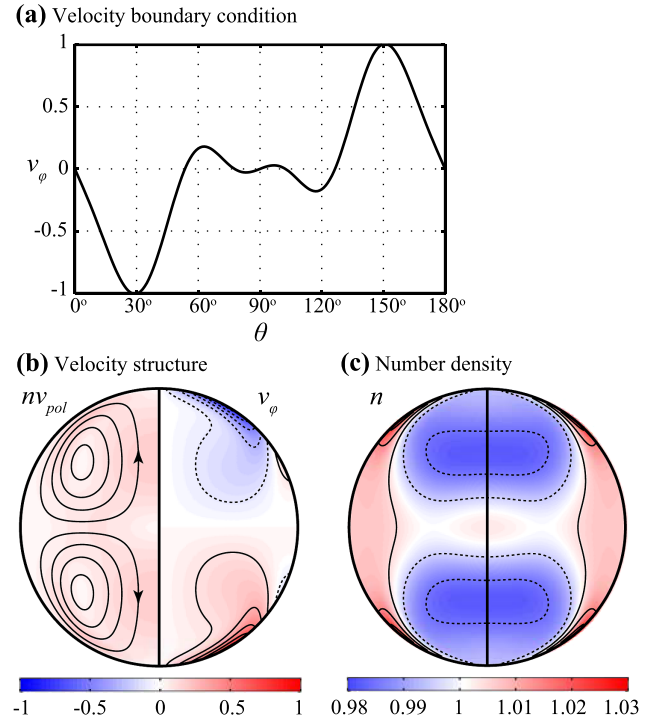


FIG. 2. Axisymmetric equilibrium flow of von Kármán type for Mach number $M=1$ and fluid Reynolds number $Re=300$ used in kinematic dynamo study: (a) velocity boundary condition $v_\phi(\theta)$ adopted from Ref. 18; (b) structure of normalized velocity; (c) contour plot of normalized density (dashed lines denote $n < 1$). Left half of (b) shows stream lines of poloidal flux nv_{pol} superimposed on its absolute values depicted in colors; right half of (b) shows contour plot of azimuthal velocity v_ϕ (dashed lines denote $v_\phi < 0$). Vertical lines in (b) and (c) represent the axis of symmetry.

$Re=300$, and the magnetic Reynolds numbers up to $Rm=400$. These parameters can be achieved in MPDX by creating an argon plasma with $V_0 = 5 \text{ km/s}$, $n_0 = 10^{18} \text{ m}^{-3}$, $T_e = 10 \text{ eV}$, and $T_i = 1 \text{ eV}$.

In the NIMROD simulation, we used a meshing of the poloidal plane with 4608 quadrilateral finite elements of polynomial degree 2 and 6 Fourier harmonics in the ϕ -direction (the azimuthal mode numbers are $0 \leq m \leq 5$). This resolution was sufficient for the laminar flow under consideration. We took a non-moving fluid ($\mathbf{v} = 0$) with uniform density ($n = 1$) as the initial state and evolved Eqs. (1)–(3) until a steady state was reached. The resulting velocity field $\mathbf{v}(r, \theta)$ (Fig. 2) is axisymmetric and hydrodynamically stable with respect to perturbations with $m > 0$.

The main results of the paper are obtained by solving the kinematic dynamo problem with this velocity field,

$$\gamma \mathbf{B} = Rm \nabla \times (\mathbf{v} \times \mathbf{B}) + \nabla^2 \mathbf{B}, \quad \nabla \cdot \mathbf{B} = 0, \quad (4)$$

for unknown magnetic field \mathbf{B} and normalized dynamo growth rate $\gamma = \Gamma R_0^2 / \eta$. We represent the divergence-free field as an expansion in a spherical harmonic basis²³

$$\mathbf{B} = \nabla \times \nabla \times \left[\sum_{l=m}^L S_l Y_l^m \mathbf{e}_r \right] + \nabla \times \left[\sum_{l=m}^L T_l Y_l^m \mathbf{e}_r \right], \quad (5)$$

where $S_l(r)$ and $T_l(r)$ are functions of r only and Y_l^m are spherical harmonics related to the associated Legendre

polynomials by $Y_l^m(\theta, \phi) = P_l^m(\cos \theta)e^{im\phi}$. Since the velocity is axisymmetric, we consider each azimuthal mode m separately. The summation in Eq. (5) is truncated at some L ($L = 20$ provides a satisfactory convergence in these studies). Substituting Eq. (5) into Eq. (4) and using the orthogonality of spherical harmonics, one obtains for $m \leq l \leq L$

$$\gamma S_l = \frac{\partial^2 S_l}{\partial r^2} - \frac{l(l+1)S_l}{r^2} + A_l^m \sum_{j=m}^L \left[I_{lj}^{(1)} S_j - I_{lj}^{(2)} \frac{\partial S_j}{\partial r} + I_{lj}^{(3)} T_j \right], \quad (6)$$

$$\begin{aligned} \gamma T_l = & \frac{\partial^2 T_l}{\partial r^2} - \frac{l(l+1)T_l}{r^2} - A_l^m \sum_{j=m}^L \left[\overline{I_{jl}^{(1)}} T_j \right. \\ & \left. + \frac{\partial}{\partial r} \left(I_{lj}^{(2)} T_j + I_{lj}^{(3)} \frac{\partial S_j}{\partial r} + I_{lj}^{(4)} S_j \right) + \overline{I_{jl}^{(4)}} \frac{\partial S_j}{\partial r} \right]. \quad (7) \end{aligned}$$

Here, the bar above a symbol denotes its complex conjugate, A_l^m is a numerical factor

$$A_l^m = Rm \frac{(2l+1)(l-m)!}{2l(l+1)(l+m)!}$$

and $I_{lj}^{(1-4)}(r)$ are functions of r given by the integrals

$$I_{lj}^{(1)} = \frac{j(j+1)}{r} \int_0^\pi \overline{Y_j^m} \left[v_\theta \frac{\partial Y_l^m}{\partial \theta} \sin \theta - imv_\phi Y_l^m \right] d\theta,$$

$$I_{lj}^{(2)} = \int_0^\pi v_r \left[\frac{\partial Y_l^m}{\partial \theta} \frac{\partial \overline{Y_j^m}}{\partial \theta} \sin \theta + \frac{m^2 Y_l^m \overline{Y_j^m}}{\sin \theta} \right] d\theta,$$

$$I_{lj}^{(3)} = im \int_0^\pi \frac{\partial v_r}{\partial \theta} Y_l^m \overline{Y_j^m} d\theta,$$

$$I_{lj}^{(4)} = \frac{j(j+1)}{r} \int_0^\pi \overline{Y_j^m} \left[v_\phi \frac{\partial Y_l^m}{\partial \theta} \sin \theta + imv_\theta Y_l^m \right] d\theta.$$

To calculate these integrals, we interpolate the velocity field on a uniform polar grid (typically with $N_r = 50$ radial and $N_\theta = 1000$ angle grid points) and use the trapezoidal rule.

Equations (6) and (7) should be supplemented with boundary conditions for functions $S_l(r)$ and $T_l(r)$. The regularity of the field at the center of the sphere requires

$$S_l|_{r=0} = 0, \quad T_l|_{r=0} = 0. \quad (8)$$

The outer boundary conditions depend on the properties of the shell. To avoid undesired diversion of flow-driving current into the shell, the inner surface in MPDX is covered with an insulating coating (Fig. 1(c)). Thus, the normal component of current is zero at $r = 1$, i.e.,

$$T_l|_{r=1} = 0. \quad (9)$$

To derive the condition for S_l at $r = 1$, we consider the model shown in Fig. 1(c) and use the general boundary condi-

tions for normal and tangential components of the magnetic field at the interface between two media with different relative magnetic permeabilities μ_1 and μ_2 : $B_{1n} = B_{2n}$, $B_{1t}/\mu_1 = B_{2t}/\mu_2$. We also assume that the insulating coating is thin enough that it has no impact on profile of S_l . Then the resulting equations are (omitting “ r ” in S_l)

$$r = 1 : S = S_w, \quad \frac{1}{\mu} \frac{\partial S}{\partial r} = \frac{1}{\mu_w} \frac{\partial S_w}{\partial r}, \quad (10)$$

$$1 < r < 1 + \frac{d}{R_0} : \frac{\eta}{R_0} \gamma S_w = \frac{\partial^2 S_w}{\partial r^2} - \frac{l(l+1)S_w}{r^2}, \quad (11)$$

$$r = 1 + \frac{d}{R_0} : S_w = S_v, \quad \frac{1}{\mu_w} \frac{\partial S_w}{\partial r} = \frac{\partial S_v}{\partial r}, \quad (12)$$

$$r > 1 + \frac{d}{R_0} : S_v \propto r^{-l}, \quad (13)$$

where Eq. (11) is derived for a stationary wall with thickness d , symbols with subscripts refer to wall (“ w ”) and vacuum (“ v ”), and symbols without subscript refer to plasma. We assume that the variations of S_l in the wall are small. This is the thin-wall approximation,¹⁴ it applies if $d \ll R_0$ and $d \ll |\eta_w/\Gamma|^{1/2}$. Then Eqs. (10)–(13) are reduced to

$$\left(\frac{\partial S_l}{\partial r} (1 + lc_\mu) + S_l (l\mu + \gamma c_\sigma) \right) \Big|_{r=1} = 0, \quad (14)$$

where we have used the relation $\eta = c^2/(4\pi\sigma\mu)$ between magnetic diffusivity η and electric conductivity σ (c is the

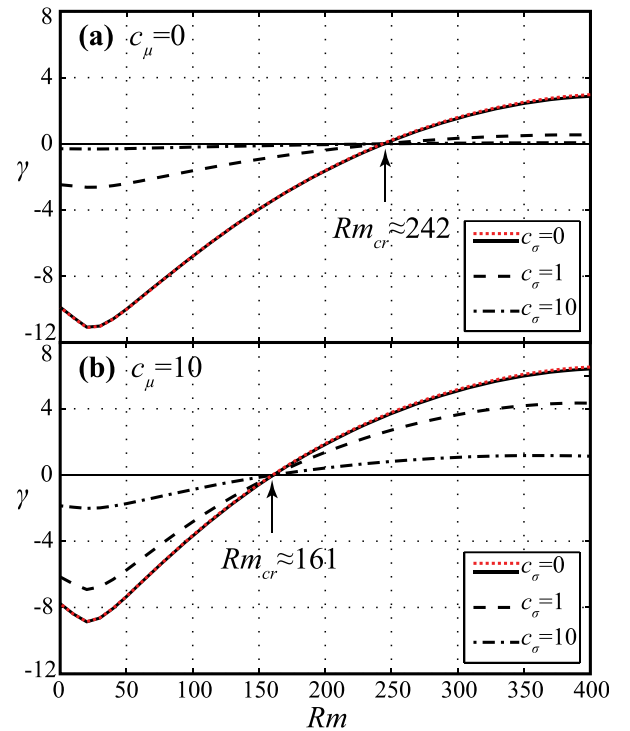


FIG. 3. Dependence of dynamo growth rate γ on magnetic Reynolds number Rm for different values of the wall parameters c_σ and c_μ . Calculations for $c_\sigma = 0$ are performed with two resolutions: $L = 20$, $N_r = 50$ (solid line) and $L = 30$, $N_r = 100$ (dotted line, almost overlapping with solid one). The cases with $c_\sigma = 1$ (dashed line) and $c_\sigma = 10$ (dashed-dotted line) are done with $L = 20$, $N_r = 50$.

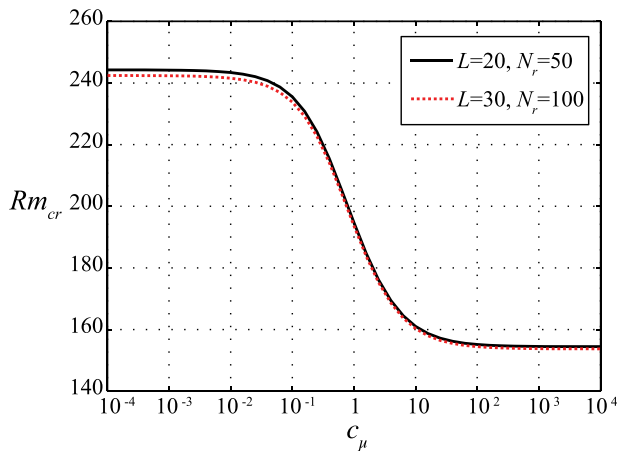


FIG. 4. Dependence of critical magnetic Reynolds number Rm_{cr} on the wall permeability parameter c_μ obtained with two resolutions: $L=20$, $N_r=50$ (solid line) and $L=30$, $N_r=100$ (dotted line).

speed of light) and introduced the wall conductivity parameter $c_\sigma = \sigma_w d / (\sigma R_0)$ and the wall permeability parameter $c_\mu = \mu_w d / R_0$. Equation (14) is obtained for a stationary wall without requiring the no-slip boundary condition for plasma velocity, in contrast to analogous equation (14) from Ref. 14.

Equations (6)–(9) and (14) constitute an eigenvalue problem for the dynamo growth rate γ and unknown eigenfunctions S_l and T_l . In order to solve it, we apply the finite difference method and discretize S_l and T_l for each harmonic l ($m \leq l \leq L$) on a uniform grid at $0 \leq r \leq 1$ with N_r equal intervals. The resulting system is cast in the form of a matrix eigenvalue equation, which is solved in MATLAB. The developed scheme has been benchmarked against the results of the kinematic dynamo studies from Refs. 24–26 (see Ref. 27 for details).

Here, we report the results of solving the kinematic dynamo eigenvalue problem with the velocity shown in Fig. 2, relative permeability of the plasma $\mu = 1$, magnetic Reynolds numbers $Rm = 0$ –400, and varying wall parameters c_σ and c_μ . We consider only the most unstable (or least decaying) $m = 1$ azimuthal mode. The results are summarized in Figs. 3 and 4. In the present case, γ is always real, so the dynamo threshold Rm_{cr} corresponds to the condition $\gamma = 0$. Rm_{cr} does not depend on the wall conductivity parameter c_σ . This is because c_σ drops out of the problem when $\gamma = 0$, as follows from Eq. (14). However, c_σ affects the dynamo growth rate: larger values of c_σ (larger wall conductivity) lead to lower $|\gamma|$. In the limit of a perfectly conducting shell, no growing field is possible, since $\gamma \rightarrow 0$.

The wall permeability parameter c_μ has a strong influence on both dynamo threshold Rm_{cr} and growth rate γ . A ferritic wall facilitates dynamo action. As shown in Fig. 4, Rm_{cr} decreases with increase of c_μ : from $Rm_{cr} \approx 242$ when $c_\mu = 0$ to $Rm_{cr} \approx 154$ when $c_\mu \rightarrow \infty$. These results are consistent with previous theoretical dynamo studies in other geometries,^{9,10,12,13} which indicated reduction of Rm_{cr} for the ferritic-wall boundary conditions.

Estimates for typical parameters of MPDX show that its wall is very conducting and non-ferritic with $c_\sigma \approx 30$ and

$c_\mu \approx 0$. Under these conditions, dynamo action is achievable for the considered flow if $Rm \gtrsim 242$, the respective dynamo growth rate at $Rm = 400$ is $\Gamma \approx 3.6 \text{ s}^{-1}$.

In summary, we have studied the influence of finite conductivity and permeability of the wall on a plasma dynamo, generated in a sphere by a compressible laminar flow of von Kármán type. Our results show that in such flow the dynamo threshold is affected only by the wall permeability, while the dynamo growth rate depends on both wall properties.

The authors wish to thank C. Sovinec for valuable help and discussions related to NIMROD.

¹N. L. Peffley, A. B. Cawthorne, and D. P. Lathrop, *Phys. Rev. E* **61**, 5287 (2000).

²C. B. Forest, R. A. Bayliss, R. D. Kendrick, M. D. Nornberg, R. O'Connell, and E. J. Spence, *Magnetohydrodynamics* **38**, 107 (2002).

³M. Bourgoïn, L. Marié, F. Pétrélis, C. Gasquet, A. Guigon, J.-B. Luciani, M. Moulin, F. Namer, J. Burguete, A. Chiffaudel, F. Daviaud, S. Fauve, Ph. Odier, and J.-F. Pinton, *Phys. Fluids* **14**, 3046 (2002).

⁴A. Gailitis, O. Lielausis, S. Dement'ev, E. Platacis, A. Cifersons, G. Gerbeth, T. Gundrum, F. Stefani, M. Christen, H. Hänel, and G. Will, *Phys. Rev. Lett.* **84**, 4365 (2000).

⁵R. Stieglitz and U. Müller, *Phys. Fluids* **13**, 561 (2001).

⁶R. Monchaux, M. Berhanu, M. Bourgoïn, M. Moulin, Ph. Odier, J.-F. Pinton, R. Volk, S. Fauve, N. Mordant, F. Pétrélis, A. Chiffaudel, F. Daviaud, B. Dubrulle, C. Gasquet, L. Marié, and F. Ravelet, *Phys. Rev. Lett.* **98**, 044502 (2007).

⁷G. Verhille, N. Plihon, M. Bourgoïn, P. Odier, and J.-F. Pinton, *New J. Phys.* **12**, 033006 (2010).

⁸M. S. Chu and M. Okabayashi, *Plasma Phys. Controlled Fusion* **52**, 123001 (2010), and references therein.

⁹R. Avalos-Zuniga, F. Plunian, and A. Gailitis, *Phys. Rev. E* **68**, 066307 (2003).

¹⁰R. Avalos-Zuniga and F. Plunian, *Eur. Phys. J. B* **47**, 127 (2005).

¹¹R. Laguerre, C. Nore, J. Léorat, and J.-L. Guermont, *C. R. Mec.* **334**, 593 (2006).

¹²C. Gissinger, A. Iskakov, S. Fauve, and E. Dormy, *Europhys. Lett.* **82**, 29001 (2008).

¹³C. Gissinger, *Europhys. Lett.* **87**, 39002 (2009).

¹⁴P. H. Roberts, G. A. Glatzmaier, and T. L. Clune, *Geophys. Astrophys. Fluid Dyn.* **104**, 207 (2010).

¹⁵C. Guervilly and P. Cardin, *Geophys. Astrophys. Fluid Dyn.* **104**, 221 (2010).

¹⁶A. Giesecke, C. Nore, F. Stefani, G. Gerbeth, J. Léorat, F. Luddens, and J.-L. Guermont, *Geophys. Astrophys. Fluid Dyn.* **104**, 505 (2010).

¹⁷C. B. Forest, R. A. Bayliss, D. D. Schnack, E. J. Spence, and K. Reuter, *Bull. Am. Phys. Soc.* **53**, 222 (2008).

¹⁸E. J. Spence, K. Reuter, and C. B. Forest, *Astrophys. J.* **700**, 470 (2009).

¹⁹C. Collins, N. Katz, J. Wallace, J. Jara-Almonte, I. Reese, E. Zweibel, and C. B. Forest, *Phys. Rev. Lett.* **108**, 115001 (2012).

²⁰S. I. Braginskii, *Reviews of Plasma Physics* (Consultants Bureau, New York, 1965), Vol. 1, p. 205.

²¹I. V. Khalzov, B. P. Brown, F. Ebrahimi, D. D. Schnack, and C. B. Forest, *Phys. Plasmas* **18**, 032110 (2011).

²²C. R. Sovinec, A. H. Glasser, T. A. Gianakon, D. C. Barnes, R. A. Nebel, S. E. Kruger, D. D. Schnack, S. J. Plimpton, A. Tarditi, M. S. Chu, and NIMROD Team, *J. Comput. Phys.* **195**, 355 (2004).

²³E. C. Bullard and H. Gellman, *Philos. Trans. R. Soc. London Ser. A* **247**, 213 (1954).

²⁴M. L. Dudley and R. W. James, *Proc. R. Soc. London Ser. A* **425**, 407 (1989).

²⁵K. Li, P. W. Livermore, and A. Jackson, *J. Comput. Phys.* **229**, 8666 (2010).

²⁶E. J. Kaplan, B. P. Brown, K. Rahbarnia, and C. B. Forest, *Phys. Rev. E* **85**, 066315 (2012).

²⁷See supplementary material at <http://dx.doi.org/10.1063/1.4757219> for details on benchmarking and convergence study of our numerical scheme.